THE FORMATION OF OPAL IN MARINE REPTILE BONES AND WOOD

BENJAMATH PEWKLIANG[1,2], ALLAN PRING[1,2], AND **JÖEL BRUGGER[1,2]**

[1]*School of Earth & Environmental Sciences, Discipline of Geology & Geophysics, University of Adelaide, Adelaide 5000, South Australia, Australia*

[2]*Department of Mineralogy, South Australian Museum, North Terrace, Adelaide 5000, South Australia, Australia*

2004.

CONTENTS

THE FORMATION OF OPAL IN MARINE REPTILE BONES AND WOOD

BENJAMATH PEWKLIANG[1,2], ALLAN PRING[1,2], AND **JÖEL BRUGGER[1,2]**

[1]*School of Earth & Environmental Sciences, Discipline of Geology & Geophysics, University of Adelaide, Adelaide 5000, South Australia, Australia*

[2]*Department of Mineralogy, South Australian Museum, North Terrace, Adelaide 5000, South Australia, Australia*

email: benjamath.pewkliang@adelaide.edu.au

KEYWORDS: opal, wood, bone, plesiosaur, ichthyosaur

ABSTRACT

The age of precious opal and the mechanisms that result in formation as opposed to the ubiquitous common opal, are poorly understood. Until now, there has been no research on the replacement of biominerals in vertebrate bones by opal. As the microtexture, mineralogy and chemistry of bones are well-known, they provide a unique opportunity to study the mechanism of precious opal deposition. In this article chemical and textural features of Andamooka opalised plesiosaur bones were compared with those in non-

opalised ichthyosaur bones from Moon Plain and a recent dolphin bone. Opalised wood samples from Nevada and White Cliffs were also studied, to compare with bone opalisation and different depositional environments (sedimentary vs volcanogenic).

The cellular form of a continuous irregular framework of silica was retained in the wood samples. The mineralogy of the wood samples reflects their depositional environment, where opal-CT and opal-C is dominant in volcanic deposits (Nevada) and opal-A in sedimentary deposits (White Cliffs). Comparison of the Nevada wood to Post Archean average shale (PAAS) shows that it is rich in most trace elements, with the exception of Y and U. The high amount of trace elements is a reflection of its volcanic origin. In contrast, the opalised wood from White Cliff is depleted in most trace elements, with the exception of Co.

Cracks were observed in both the opalised wood and bone samples which allowed the void space required to form precious opal. The opalised wood from White Cliffs and the opalised plesiosaur bones from Andamooka are chemically very similar and reflect similar compositions for the opalising fluids.

The Haversian system was preserved in the non-opalised ichthyosaur bone, but not in the opalised bones. The ichthyosaur bone has comprises mostly of carbonatehydroxylapatite, but in the opalised bones, the major mineral is quartz. Modern dolphin bone consists of bioapatite with water and organic material, and its trace element composition is broadly similar to the ichthyosaur bone from Moon Plain, but is richer in Sr, Zn and Co. When

normalized to PAAS, the ichthyosaur bone is depleted in all trace elements with the exception of Sr, which is likely a product of the carbonate-rich mineralogy. Like the ichthyosaur bones, the opalised bones are also depleted in trace elements, with the exception of Co and Zn. There is no evidence of remnant bioapatite in the opalised bone, a finding consistent with the chemical analyses that show only trace amounts of Ca and no P. The level of microstructural preservation in the opalised bone suggests that opalisation is not a closely coupled dissolution–reprecipitation reaction and that there was a fluid filled space between the reaction fronts which allowed the opal silica spheres to form and settle within a comparatively small space (100 μm). An alternative interpretation is that the fibrous quartz filled the osteon canals before opalisation and that the bioapatite was then dissolved away leaving a hollow cast that filled slowly with opal.

INTRODUCTION

The nature of precious opal

Opal, which has a chemical composition of $SiO_2.nH_2O$, are divided into two forms: microcrystalline and non-crystalline. Microcrystalline opals consist of opal-CT (tridymite) and opal-C (cristobalite). The former is based on layers of cristobalite/tridymite with strong stacking disorder while the later has disordered low-cristobalite with minor evidence for tridymitic stacking (Jones and Segnit 1971). Non-crystalline opal consists of opal-A, opal-AN and opal-AG. Opal-A is a biogenic form of silica whereas opal-AN (hyalite) is water containing amorphous (network-forming) silica glass (Flörke et al 1973). In contrast,

opal-AG is the form found in precious (play of colour) and potch opal (no play of colour). Opal-AG is an ordered arrangement of non-crystalline amorphous gel-like aggregate of spherical silica sphere and water filling the interstices (Jones et al 1964). It is the ordering of the silica spheres that causes the play of colour seen in precious opals. This is due to the fact they have different refraction indices and thus the size of spheres and orientation of crystal-like packing determines which colour is visible (Sanders 1968). A colour change is observed in the fracture surface along grain boundaries as the angle of incidence of light is changed. The grain boundaries in natural opal are sharp and straight sided which allows for a uniform texture in each colour domain. In contrast, synthetic opals have apparent crenulated boundaries and sub-grains can be seen inside most colour grains to cause the lizard skin colour of play (Fig. 2a). Although both forms contain variable amounts of non-essential water, the minerals are usually rather pure and non-volatile impurities are below 1 mol % in most samples and often even below 0.5 mol % (Graetsch 1994).

Genesis of precious opal

The processes leading to the formation of precious opal and the opalisation of fossils in Australian opal deposits are poorly understood. There is considerable debate about the age of the opal. Barker (1980) and others concluded that opalisation occurred in the Late Cretaceous. Horton (2002), however, proposes that opal deposition occurred after gentle warping 24 Ma ago and thus much later than the deposition of the Cretaceous sediments in which it is found. In contrast, ^{14}C dating of black opal from Lightning Ridge reveals Quaternary ages for the organic matter in these opals (Dowell and Mavrogenes 2004).

There has also been debate about the source of the silica, the composition of the opalising fluids and the mechanism of precious opal formation in the Australian deposits (see Barnes et al 1992 for overview). In much of the world, precious opal is formed from volcanic fluids. Indeed volcanic opal is a very common phase resulting from hydrothermal alteration of felsic volcanics by acid sulfate fluids and from the boiling and/or mixing of neutral chloride geothermal brines in epithermal settings (Corbett and Leach 1998). It has been suggested that the formation of precious opal requires the amorphous silica to slowly settle out of a dilute water solution (Darragh et al 1976). In Australia, which produces 95% of the world's reserves, precious opal occurs over a wide area (Horton 2002) in veins and nodules within clay layers in shales and sandstones with no volcanogenic input. Three models for the origin of precious opal in Australia have been proposed: (1) the weathering model (e.g., Senior 1988), (2) the syntectonic model (refer to Pecover 1996 for overview) and (3) the microbial model (e.g. Behr et al 2000). Precious and potch opal are also found replacing shells, wood and less frequently, the bones and teeth of marine reptiles (Barnes et al 1992). Partially or completely opalised skeletons of Cretaceous plesiosaurs and ichthyosaurs have been found at Andamooka, Coober Pedy and White Cliffs (Fig. 1; Kear 2003).

Opalisation of bones and wood

Ichthyosaurs were dolphin-like marine reptiles that lived during the Mesozoic. By making the outer layers of their bones spongy and less dense, modern deep-diving mammals can enhance the strength needed to support the body while being fairly buoyant (Fig. 2f; Motani

2004). The same type of spongy layer also encases the bones of ichthyosaurs, creating lighter skeletons (Motani 2004). Like dolphins, the structural features such as the Haversian systems, primary osteons, laminae, osteocyte lacunae (with adjoining canaliculi) and growth rings are preserved. At its very simplest, the Haversian system or the osteon (a network of canals and tubes which provide blood supply to the cells within the fibrous bone structure) is 200 μm in diameter (Blystone 1999). The variation in diameter can be due to the age of the osteon and its relative position within the bone.

It is reported that the silicification of plant material is not a replacement but a permineralization where the organic structure acts as a template for silica deposition (Carson 1991). Siliceous skeletons such as wood are mainly composed of opaline silica (opal A), which contains up to 10% water (Tucker 1991). The silicification of wood occurs as the concentration of silica increases with burial-time and the concentration of water diminishes. With time, the abundance of opaline silica decreases as it transforms to quartz (Fig. 3). Diagenetic modification of opal-A mostly proceeds in the direction of opal-A to opal-CT to quartz and opal-A to quartz. The transformation from opal-CT to quartz is a solution reprecipitation reaction that may occur due to increases in temperature and pressure due to depth of burial or due to kinetic effects involving a mineralizing agent, such as organic matter or carbonate ions (Carson 1991). The change from opal-A to quartz is reported to occur when sediment pore waters is undersaturated with respect to opal-A and supersaturated with respect to quartz. In contrast, the opal-A to opal-CT and opal-A to quartz transitions involve a dissolution-reprecipitation reaction (Carson 1991). As opal-A is transformed to opal-CT, the later becomes progressively ordered and the $d_{(101)}$ spacing of

cristobalite decreases (Kano 1983). The structure of the wood preserved is an indicator that a certain amount of structural degradation is necessary to allow silicification to take place, but that preservation of structures associated with soft tissues indicates that silicification took place prior to significant decay.

Objectives

The process of mineralisation of bone and wood for preservation in the fossil record is dependant on the chemical and physical conditions during diagenesis, particularly the composition of the mineralizing fluid. Fundamentally these processes can be considered as mineral replacement reactions, where the biomineral is replaced by another mineral such as quartz, opal or calcite. The replacement reaction can also be associated with recrystallisation of the biomineral, particularly bioapatite, during which trace amounts of heavy metals may be incorporated into its structure (Hubert et al 1996). Using the analogy in bone structure of modern dolphin bone with that of ichthyosaur and plesiosaur, the diagenetic changes that transformed bioapatite (carbonatehydroxylapatite) to opal-AG will be documented (Sanders 1964). The opalised bones are three-dimensional replicas of ancient biogenic objects which have been transformed into non-precious potch or rare and valuable precious opal. For the very fine scale microstructure of the fossil to be preserved the dissolution reaction that dissolves the biomineral must be tightly coupled to the precipitation reaction, so that no free space occurs at the reaction front (Putnis 2002). Such replacement reactions therefore proceed as the fluid fronts move through the fossil. If the dissolution and precipitation reactions are not tightly coupled and there is a gap between the

dissolution front and the precipitation front fine details of the microstructure will not be preserved. The maturation of the silica cell wall in wood to form opal will be examined in fossilized wood from Coober Pedy, volcanogenic opalised wood from Nevada and opalised wood from White Cliff.

We report the results of a detailed investigation of the chemistry, structure and microstructure of opalised marine reptile bones from Andamooka and Coober Pedy and opalised wood from White Cliffs. This material is compared to opalised wood from Nevada and ichthyosaur bone from the same geological unit near Coober Pedy, which has not been opalised.

LOCATION AND SETTING

The opalised fossils at Coober Pedy and Andamooka are found within the opal-bearing layers of the Bulldog Shale (Barremian-Early Albian), whereas at White Cliffs they are found within the Doncaster Member of the Wallumbilla Formation (Late Barremian-Aptian). When fresh, the Bulldog Shale is a dark grey, silty and sandy, smectite-rich claystone with lenses of sand, limestone and occasional erratic boulders. In contrast, the weathered Bulldog shale (the host rock for opal) comprises bleached, porous, kaolinitic claystone overlying darker, denser, smectitic claystone (Robertson and Scott 1990). Both precious and potch opal are found in the weathered Bulldog Shale as subhorizontal to subvertical veins infilling cracks and joints and occasionally replacing fossils. The stratigraphy and geology of Andamooka and Coober Pedy are similar and opal is

commonly found as horizontal beds known as the opal level (Fig. 4; Jones and Segnit 1966). Opal veins cutting across the opal level and pore fillings in a band of clay and conglomerate within the Bulldog Shale are also common. Opal is found at depths as great as 40 m and also on the surface level, where it has been exposed by post-Tertiary erosion. On the basis of these occurrences, opalisation has been thought to have occurred during the Tertiary period where the climatic conditions were not greatly different from those at present (Darragh et al 1966; Townsend 1976).

DEPOSITIONAL FRAMEWORK

Coober Pedy lies on the boundaries of the Permian Archaringa Basin and the Jurassic-Cretaceous Eromanga Basin. The latter is a part of the Great Artesian Basin, and was covered by a shallow sea during the early and middle Cretaceous (Aptian-Albian)(Fig. 1). Over this period the area of the Eromanga Basin received remarkably uniform, fine grained, terrigenous sediments and the northern and eastern margins of the Eromanga Basin accumulated mud, silts and very fine sands 2,000 feet in thickness, which have lain virtually undisturbed since the Cretaceous (Day 1969). The Cretaceous had two different climatic modes: a cool mode from the middle Jurassic to early Cretaceous and a warm mode from late Cretaceous to early Tertiary, which was initiated by the breakup of Pangaea in the early Cretaceous (Frakes et al 1992). The Aptian-Albian period has been defined as an ocean anoxic event, a time of oxygen-poor bottom waters in which organic matter was preserved in large quantities. Frakes et al. (1992) noted that the Aptian was a period of warming which peaked during the Albian. The marine transgression reached its peak in the

late Aptian. De Lurio and Frakes (1999) have suggested that the epicontinental seaway in which the Bulldog Shale was deposited in a highly alkaline, cold, hyposaline and oxygen-depleted environment. The occurrence of plesiosaur and ichthyosaur bones and wood at Andamooka is further evidence of a shallow, epicontinental sea that covered much of Australia, dividing it up into a series of islands (Rich and Rich 1985). At present, the Great Artesian Basin is one of the largest freshwater basins in the world and would be dominated by Ca and HCO_3. The transition from marine to freshwater replaces the Ca with Na on the exchange sites and leaves $NaHCO_3$ rich water. The composition of the water is important in the formation of opal. The climate provides alternating wet and dry periods, creating oscilating rising and falling water table which concentrates silica in solution. As rain infiltrates the soil and reacts with the minerals in the rocks, base cations are released to form silica and white kaolin. To provide the unique situation for the production of precious opal a special condition must also prevail to slow down a falling water table.

SAMPLES AND METHODS

Details of the samples examined in this study are summarized in Table 1. Polished thin sections and polished blocks of an opalised shell, 4 wood and 8 bones were examined. Of the bone samples, 5 were opalised plesiosaur bones, 2 were ichthyosaur bones and a dolphin rib. The wood samples were made up of a sedimentary opalised wood sample, a silicified wood and three opalised wood samples from a volcanic environment.

A HUBER Imaging Plate Guinier X-ray Camera model G670 was used for powder x-ray diffraction analysis. The samples were run using Co$K\alpha 1$: 1.78892Å for 10 minutes at 35 kilovolts and 34 mA. The image plate was read 6 times and each scan was averaged.

Images of the surface of the polished blocks and polished thin sections were obtained with a PHILIPS XL30 Field Emission Gun Scanning Electron Microscope (SEM). To obtain SEM images of the silica spheres in opal, some of the polished blocks were etched in a solution of 10M hydrofluoric acid for 30 seconds. Images of the carbon coated samples (to produce a conducting surface and to ensure good secondary electron emission) were obtained by using both the backscatter detector and secondary detector at either 10 kV or 15 kV. Energy dispersive X-ray spectroscopy (EDS) spectra were also collected for mineral identification purpose.

The CAMECA SX51 Electron Microprobe was used for quantitative micro-chemical analyses and qualitative x-ray elemental mapping. The carbon coated thin sections were imaged in backscattered electron mode, which highlights areas with different average atomic weights. As the major contrasts in gray levels can not be equated with each other or calibrated to specific average atomic weights, the composition of the minerals were determined by the electron microprobe. The procedure was carried out at an accelerating potential of 15 kV, a 15 nA beam current measured at a Faraday cup, and beam diameter of 2-3 μm. The standards used for elemental analyses were: Na (albite), Mg (dolomite), Al (almandine), Si (almandine), P (fluorapatite), S (pendlandite), K (sanidine), Ca (dolomite),

Cr (Cr_2O_3), Mn (rhondonite), Fe (almandine), Ni (pendlandite), Zn (sphalerite) and for trace elements Sr (celestite), V (pure vanadium), Ti (rutile), Pb (crocoite), Th (pure thorium) and U (pure uranium). Counting times of 10 seconds were used.

The bulk major and trace element compositions were measured using a PHILIPS PW 1480 X-ray fluorescence spectrometre (XRF). A pressed powder disc was used for trace element analysis and a fused disc was used for major element analysis. The fused disc was prepared by heating a mixture of sample and borate flux in a platinum alloy crucible at a high temperature (950-1250°C). During this process, the crucible was continuously agitated and a wetting agent was added every 5 minutes for the duration of time required for melting. Once the sample was completely melted, it was poured into a pre-heated circular mould and allowed to cool to produce a flat borate disc. In contrast, the pressed powdered discs were prepared by mixing and pressing the powdered sample with a binder (boric acid).

RESULTS

X-ray diffraction data

The X-ray diffraction traces for the bone samples are shown in Figure 5. The characteristic broad reflections for carbonatehydroxylapatite (bioapatite) are shown in the X-ray diffraction pattern of modern dolphin bone (N). These bioapatite reflections are also present in the diffraction pattern for the ichthyosaur limb bone from Moon Plain (G), but the reflections are somewhat sharper indicating that the bioapatite crystals may have

recrystallised during diagenesis. This diffraction trace is dominated by the sharp reflections from magnesian calcite, indicating partial replacement by magnesian calcite. The magnesian calcite fills the central canals of the osteons and probably also impregnates the carbonatehydroxylapatite in the osteon microstructure (Fig 6a, c, e).

The X-ray diffraction patterns for the three opalised plesiosaur bones (I, K and M) are all very similar and are dominated by the sharp reflections of quartz, with the three strongest lines being at 24.27° (4.255 Å), 31.06° (3.343 Å) and 59.58° (1.802 Å). Note, however, the wide hump in the background between 2θ 22 ° and 30°, relates to the amorphous structure of opal-A. This feature is somewhat less prominent in the plesiosaur limb/rib bone pattern (M). There is no evidence of remnant bioapatite in these patterns, a finding consistent with the chemical analyses that show only trace amounts of Ca and no P. The bones have been completely replaced by opal and quartz with small amounts of clay minerals sometimes trapped in the osteon canals. The opal replaces the concentric fibrous structure of the osteons, with quartz in-filling the canals (Fig. 6b, d, f).

The X-ray diffraction pattern of the opalised wood from Nevada (C) shows strong reflections due to opal-CT (tridymite opal), and its presence is consistent with the volcanic origins for this opalisation. The x-ray diffraction pattern for the opalised wood from White Cliffs (E) corresponds to opal-A and shows no evidence of reflections due to quartz (Fig. 7).

Major and trace element composition

The results of the major and trace element analyses for the samples are summarized in Table 2. The elemental analyses show that the opalised bone and wood are essentially pure SiO_2 with minor amounts of Al_2O_3 (probably present as clay inclusions) and the opalised bone samples contain no P to indicate remnant bioapatite. This is consistent with the bone structure having been completely opalised. The trace element analysis, when normalized to PAAS, shows that the bone is depleted in most trace elements, with the exception of Zr (Fig. 8). The opalised plesiosaur neural arch bone is rich in Co and Zr while the miscellaneous fragment is rich in Co, Zr and Zn. Positive correlation between Zr and Al_2O_3 supports the detrital source of these elements.

In contrast the ichthyosaur bone from Moon Plain (E) that has not been opalised, consists of bioapatite and high magnesium calcite, with only a small amount of quartz. Trace element analyses of the sample, when normalized to PAAS, also show that the ichthyosaur bone is depleted in all trace elements with the exception of Sr (Fig. 8). The elevated Sr level is probably a product of the carbonate-rich mineralogy.

The trace element patterns of these opalised samples of bone and wood from Australian fields can be contrasted with samples of opalised wood from Nevada (Fig. 9). The Nevada opalised wood shows enrichment in U, as it has 48.1 ppm compared to 0.2 ppm. With the exception of Y and U, comparison of the Nevada wood to PAAS, shows that it is rich in most trace elements. The high amount of trace element is a reflection of its volcanic origin.

In contrast, the opalised wood from White Cliff is depleted in most trace elements, with the exception of Co. As the opalised bones are also enriched in Co then the condition that formed opal is similar. The bulk composition of modern dolphin bone shows that it consists of bioapatite with water and organic material and trace element composition is broadly similar to the ichthyosaur bone from Moon Plain, but is richer in Sr, Zn and Co (Fig 8).

The opalised wood from White Cliffs and the opalised plesiosaur bones from Andamooka are chemically very similar and reflect similar compositions for the opalising fluids. Differences in mineralogy, the presence of quartz in the opalised bone filling the osteon canals and the lack of quartz in the wood indicates that the process of opalisation may have been different between the two materials. Near the fracture, which has been totally replaced by opal, the cell microstructure in the wood has not been preserved during opalisation: in this material it appears that precious opal has filled open cavities.

Opaque replacement minerals

Minor amounts of opaque replacement minerals, identified by EDS and optical properties in reflected light microscopy as chalcopyrite, pyrite and uraninite, are found in the samples. Uraninite is only found in the opalised bone samples. Both pyrite and chalcopyrite are found in the opalised bone and opalised wood samples. In the opalised bone samples, they are commonly found replacing the dense and calcareous bone along the cracks. In the opalised wood specimen, they are found within the cell structure of the wood. However,

examination of the silificed wood specimen shows that the majority of the opaque mineral, in this case pyrite, is mainly located on the outermost edge of the cell structure (Fig. 10a).

Texture preservation

The opalised wood from White Cliff and Nevada both showed that the cellular form was retained and that the cell walls are composed of a continuous irregular framework of silica coated with silica spheres (Fig. 10b, 10e). The wood sample from White Cliff had a fracture, and was found to be completely composed of precious opal silica balls (Fig. 10d). Near the fracture, the cell wall was quite rich in silica but further away, it generally retained its cell structure (Fig. 10c). It was also found to be quite porous and richer in iron than those from Nevada. In contrast, the opalised wood from Nevada had very few opal silica spheres, but was found to be rich in tabular crystals of opal-CT (Fig. 10f).

The microstructure of the calcified ichthyosaur bone (sample G) is shown in Figure 6a. The outlines of the osteons with their central canals, around 400 μm in diameter, are clear. The osteon canals are filled with magnesian calcite. The fine details of the concentric rings of bioapatite lamella and the black lacuna within the osteons are also preserved.

In both the opalised wood and bone samples, the arrangement of the silica balls was uniform. In the samples examined, the highly opalised area showed the spherical particles

to be arranged in a cubic array (refer to Ball and Malin 1973; Darragh et al 1976 for overview).

INTERPRETATIONS AND DISCUSSION

Fossil-bone francolite

Although there are changes in the chemistry and the mineral structure becomes more stoichiometric, bones are relatively stable in most diagenetic environments. The more mature the bone becomes with increasing diagenesis, the higher the concentration of phosphate and fluorine, also the larger pores are usually filled with francolite cement (Tucker 1991). Comparison of the opalised bones with the ichthyosaur bone from Moon Plain (G) and the dolphin bone (N) shows it that the former is depleted in phosphate. This is a reversal to the above statement. The reason behind the depletion in the phosphate content may be due to the depositional environment of the fossil bone. It is known that Moon Plain has a vast resource of opalised fossils. The locality was a part of the marine Eromanga Basin which teemed with marine life allowing it to become one of the best cold water Cretaceous marine deposits in the world. As water made its way into the fossil, chemical reactions occurred between the bone and water which removed the bioapatite and deposited a carbonate solution and later throughout diagenesis, trace elements.

Opalised bone and wood

The XRD trace for the Nevada wood samples indicates the presence of tridymite and cristobalite. This corresponds to opal-CT and opal-C, which is only found associated with lava flows (Segnit et al 1970; Graetsch 1994). The Nevada wood has undergone a dissolution-reprecipitaiton reaction which transformed biogenic opal-A to opal-CT (Carson 1991). The richness in opal-CT reflects the silica source from either associated magmatic waters or volcanic tuffs. The preservation of the cell wall in both the samples from White Cliffs and Nevada indicates that fossilization occurred before the cavity was filled by the silica solution. The open crack in the wood sample from White Cliff provided the space required for precipitation of the silica from feldspar by groundwater (Sanders and Darragh 1971). The silica skeleton of wood contains water, which is found in biogenic opal-A (Jones and Renaut 2004). The microstructure of opalised wood samples reflects their depositional environment.

As synthetic opals also display the cubic array of the silica spheres found in the opalised samples, one can be certain that the principle of the formation of the opal spheres is retained (refer to Smallwood 2003 for a detailed discussion). However, in the opalised bone samples, some loosely packed spheres lay in the bone cavity (Fig. 2e). The formation of opals will only occur if there are voids or porosity to provide a site for opal deposition. Although more dominant in sedimentary than volcanic rocks, the voids are created by cracks. In the opalised bone, there are both large and small scale fractures which could

have developed in response to compaction. The formation of opal in the opalised bone favours the weathering model for opal genesis in rocks of the Great Artesian Basin.

The Haversian system is preserved in the fossilized but not opalised ichthyosaur bones from the Bulldog Shale. In contrast, the opalised plesiosaur bones only show outlines of where the Haversian system may have been located. The Haversian system has been replaced with what seems like growth rings (Fig. 2b). The absence of fractures through these rings suggest that it may have resulted from diagenesis. The silica in the water would have slowly made its way into the Haversian structure and thus would produce these rings.

Biominerals has filled the Haversian system of the opalised bones along fractures as shown by SE images on unetched samples (Fig. 2b). Etched samples have shown the presence of kaolinite roses (Fig. 2d). Thus the cracks provided the space needed for silica to be deposited. Small amounts of pyrite in the samples imply that that it was deposited in acidic conditions. As there are detrital clay minerals present in some of the apatite structure then this would explain the high concentration of Al. The absence of spongy bone and minor amounts of heavy metals in the opalised bone suggest that opalisation occurred after fossilization.

The fine details of the osteons in the calcified ichthyosaur bone are preserved. This indicates that the crystallization of the bioapatite and the possible in-filling of gaps between the lamella occurred as tightly coupled reactions. The fluids moving though the canals that were later filled with magnesian calcite. Figure 6b shows the microstructure of one of the

opalised plesiosaur bones. Again the individual osteons and their central canals are clear, but much of the fine structure, such as the concentric rings of lamella and the lacuna, have not been preserved. The central canals are filled with fibrous quartz indicating that it may have crystallized from a gel filling the canals. The level of microstructural preservation in the opalised bone suggests that opalisation is not a closely coupled dissolution–reprecipitation reaction and that there was a fluid filled space between the reaction fronts. If we assume that the opalisation occurs before the canals are filled with quartz then the width of this gap between the dissolution front and the precipitation fronts must have been less than 100 μm. This distance is estimated on the level of microstructural detail that was preserved. Thus the opal silica spheres, that are around 0.3 μm in diameter (Fig. 2c) must have formed and 'settled' within a comparatively small space. They did not form and then gently settle from solution as they do in synthetically grown opal (Darragh et al 1977). The lack of fine scale features of the microstructure (concentric rings of lamella and the lacuna) is also consistent with the formation of a gel that then solidified into an array of silica spheres.

An alternative interpretation is that the fibrous quartz-filled the osteon canals before opalisation and that the bioapatite was then dissolved away leaving a hollow cast that filled slowly with opal. The problem with this alternative interpretation is that if quartz filled the canals before opalisation, it would be reasonable to expect that the quartz would also have at least partially impregnated the fibrous bioapatite structure, but this has not been observed. We currently favour the former explanation over the latter, but more detailed

studies are required before any firm conclusion can be drawn. Collection of rare earth element, isotope dating and groundwater data may constitute a better understanding of the biomineralisation and opalisation of bone and wood.

CONCLUSIONS

Analysis of the opalised bone and wood samples has led to the following conclusions:

- The diffractograms of ichthyosaur bone and dolphin bone is dominated by carbonatehydroxylapatite peaks and that of opalised bones are dominated by quartz.
- The ichthyosaur bone from Moon Plain and the opalised bones, are depleted in most trace elements relative to PAAS.
- The presence of quartz in the opalised bone filling the osteon canals and the lack of quartz in the wood indicates that the processes of opalisation may have been different for these two materials.
- Compared to the opalised wood from Nevada, the opalised wood from White Cliff is depleted in trace elements.
- The depositional environment of opal is reflected in its mineralogy where opal-C and opal-CT indicated volcanic origin and opal-A indicated sedimentary origin.
- We propose two mechanisms for the opalisation of bones
    i) opal silica spheres must have formed and 'settled' within a comparatively small space or

ii) the fibrous quartz filled the osteon canals before opalisation and that the bioapatite was then dissolved away leaving a hollow cast that filled slowly with opal.

Presence of cracks and fractures in the samples allowed water to deposit silica which settled and formed opal. The opalised wood from White Cliffs and the opalised plesiosaur bones from Andamooka are chemically very similar and reflect the similar compositions for the opalising fluids.

ACKNOWLEDGEMENTS

We are grateful to Dr Benjamin Kear, from the South Australian Museum who helped pick samples from the collection at the South Australian Museum collection and for advice on the taphonomy of the marine reptiles; to the staff at the Adelaide Microscopy (Adelaide University), especially Angus Netting, for their assistance on the electron microprobe and the scanning electron microscope, to John Stanley (University of Adelaide) who helped prepare samples for XRF analysis; to David Bruce (University of Adelaide) who helped prepare samples for HF etching; to Pontifex and Associates who made the polished thin sections and to Jack Townsend who gave advice on the history of opal formation in South Australia.

REFERENCES

Ball, R.A., and Malin, A.S., 1973, Scanning electron microscopy and opals: Australian Gemmologist, v. 11, p. 16-19.

Barker, I.C., 1980, Geology of the Coober Pedy Opal Fields with special reference to the precious opal deposits [unpublished M.Sc thesis]: University of Adelaide, Adelaide.

Barnes, L.C., Townsend, I.J., Robertson, R.S., and Scott, D.C., 1992, Opal: South Australia's Gemstone: South Australia, Department of Mines and Energy.

Barnes, L.C., and Townsend, I.J., 1990 Opal deposits in Australia in Hughes, F.E., ed., Geology of mineral deposits of Australia and Papua New Guinea, Vol. 1, The Australiasian institute of mining and metallurgy, p. 77-84.

Behr, H.J., Behr, K., and Watkins, J.J., 2000, Cretaceous microbes producer of black opal at Lightning Ridge, NSW, Australia: Understanding Planet Earth: Searching for a sustainable future. Abstracts of the 15th Australian Geological Convention, p. 28.

Blystone, R.V., 1999, The Osteon: Introduction, Synergistic Learning in Biology and Statistics, Trinity University, San Antonio, Texas.

Carson, G.A., 1991, Silicification of Fossils, in Allison, P.A., and Briggs, D.E.G., eds., Taphonomy: releasing the data locked in the fossil record: New York, Plenum Press, p. 455-499.

Corbett, G.J., and Leach, T.M., 1998, Southwest Pacific rim gold-copper systems: structure, alteration, and mineralization, Society of Economic Geologists.

Darragh, P.J., Gaskin, A.J., Terrell, B.C., and Sanders, J.V., 1966, Origin of precious opal: Nature, v. 209, p. 13-16.

Darragh, P.J., Gaskin, A.J., and Sanders, J.V., 1976, Opals: Scientific American, v. 234, p. 84-95.

Darragh, P.J., Gaskin, A.J., and Sanders, J.V., 1977, Synthetic opals: Australian Gemmologist, v. 13, p. 109-118.

Day, R.W., 1969, The Lower Cretaceous of the Great Artesian Basin, in Campbell, K.S.W., ed., Stratigraphy and Palaeontology: Essays in Honour of Dorothy Hill: Canberra, Australian National University Press, p. 140-173.

De Lurio, J.L., and Frakes, L.A., 1999, Glendonites as a palaeoenvironmental tool: Implications for early Cretaceous high latitude climates in Australia: Geochimica et Cosmochimica Acta, v. 63, p. 1039-1048.

Dowell, K., and Mavrogenes, J., 2004, Black Opal, in Mcphie, J., and McGoldrick, P., eds., Geological Society of Australia Abstracts 73- Dynamic Earth: Past, Present and Future: Sydney, Geological Society of Australia Incorporated, p. 68.

Flörke, O.W., Jones, J.B., and Segnit, E.R., 1973, The genesis of hyalite: Neues Jahrbuch fur Geologie und Palaontologie, Monatshefte., p. 82-89.

Frakes, L.A., Francis, J.E., and Syktus, J.I., 1992, Climate modes of the Phanerozoic: the history of the earth's climate over the past 600 million years: Cambridge, Cambridge University Press, p. 65-98.

Graetsch, H.I., 1994, Structural characteristics of opaline and microcrystalline silica minerals, in Heaney, P.J., Prewitt, C.T., and Gibbs, G.V., eds., Silica: physical behavior, geochemistry and materials applications: Reviews in Mineralogy: Michigan, Mineralogical Society of America. Book Crafters, Inc, p. 209-232.

Horton, D., 2002, Australian sedimentary opal-Why is Australia unique?: Australian Gemmologist, v. 21, p. 287-294.

Hubert, J.K., Panish, P.T., Chure, D.J., and Prostak, K.S., 1996, Chemistry, microstructure, petrology and diagenetic model of Jurassic dinosaur bones, Dinosaur National Monument, Utah: Journal of Sedimentary Research, v. 66, p. 531-547.

Jones, J.B., Sanders, J.V., and Segnit, E.R., 1964, Structure of Opal: Science, p. 990-991.

Jones, J.B., and Segnit, E.R., 1966, The occurrence and formation of opal at Coober Pedy and Andamooka: Australian Journal of Science, v. 29, p. 129-133.

Jones, J.B., and Segnit, E.R., 1971, The nature of opal. 1. Nomenclature and constituent phases: Journal of the Geological Society of Australia, v. 18, p. 57-68.

Jones, B., and Renaut, R.W., 2004, Water content of opal-A: Implications for the origin of laminae in geyserite and sinter: Journal of Sedimentary Research, v. 74, p. 117-128.

Kano, K., 1983, Ordering of Opal-CT in diagenesis: Geochemical Journal, v. 17, p. 87-93.

Kear, B.P., 2003, Cretaceous marine reptiles of Australia: a review of taxonomy and distribution: Cretaceous Research, v. 24, p. 277-303.

Martill, D.M., 1991, Bones as stones: The contribution of vertebrate remains to the lithologic record, in Donovan, S.K., ed., The Processes of Fossilization: London, Belhaven Press.

Motani, R., 2004, Rulers of the Jurassic Seas: Scientific American Special Edition: Dinosaurs and other Monsters, v. 14, p. 4-11.

Neville, A.C., 1993, Biology of Fibrous Composites: Cambridge, U.K., Cambridge University Press.

Pecover, S.R., 1996, A new genetic model for the origin of opal in Cretaceous sediments of the Great Artesian Basin: Mesozoic geology of the eastern Australian Plate conference, p 450-454.

Putnis, A., 2002, Mineral replacement reactions: from macroscopic observations to microscopic mechanisms: Mineralogical Magazine, v. 66, p. 689-708.

Rich, P.V., and Rich, T.H., 1985, Plesiosauridae; the Andamooka sea monster, in Rich, P.V., and van Tets, G.F., eds., Kadimakara; extinct vertebrates of Australia.: Australia, Pioneer Design Studio. Lilydale, Victoria, Australia, p. 143-146.

Robertson, R.S., and Scott, D.C., 1990, Geology of the Cooper Pedy precious stones field: results of investigations, 1981-1986: Adelaide, Geological Survey, Department of Mines and Energy, South Australia.

Sanders, J.V., 1964, Colour of precious opal: Nature, v. 204, p. 1151-1153.

Sanders, J.V., 1968, Diffraction of light by opals: Acta Crystallographica, v. 24, p. 427-434.

Sanders, J.V., and Darragh, P.J., 1971, The microstructure of precious opal: The Mineralogical Record, v. 2, p. 261-268.

Segnit, E.R., Anderson, C.A., and Jones, J.B., 1970, A scanning microscope study of the morphology of opal: Search, v. 1, p. 349-351.

Senior, B.R., 1998, Weathered-profile-hosted precious opal deposits: AGSO Journal of Australian Geology & Geophysics, v. 17, p. 225-227.

Smallwood, A., 2003, 35 years on, a new look at synthetic opal: Australian Gemmologist, v. 21, p. 438-447.

Taylor, S.R., and McClennan, S.M., 1985, The Continental Crust: its Composition and Evolution: Geoscience Texts: Oxford, Blackwell Scientific Publications.

Townsend, I.J., 2001, The geology of Australian opal deposits: Australian Gemmologist, v. 21, p. 34-37.

Townsend, I.J., 1976, Stratagraphic Drilling in the Arckaringa Basin, 1969-1971. Report of Investigations, v. 45: Adelaide, Geological Survey of South Australia.

Tucker, 1991, The Diagenesis of Fossils, in Donovan, S.K., ed., Processes of Fossilization: London, Belhaven Press.

FIGURES

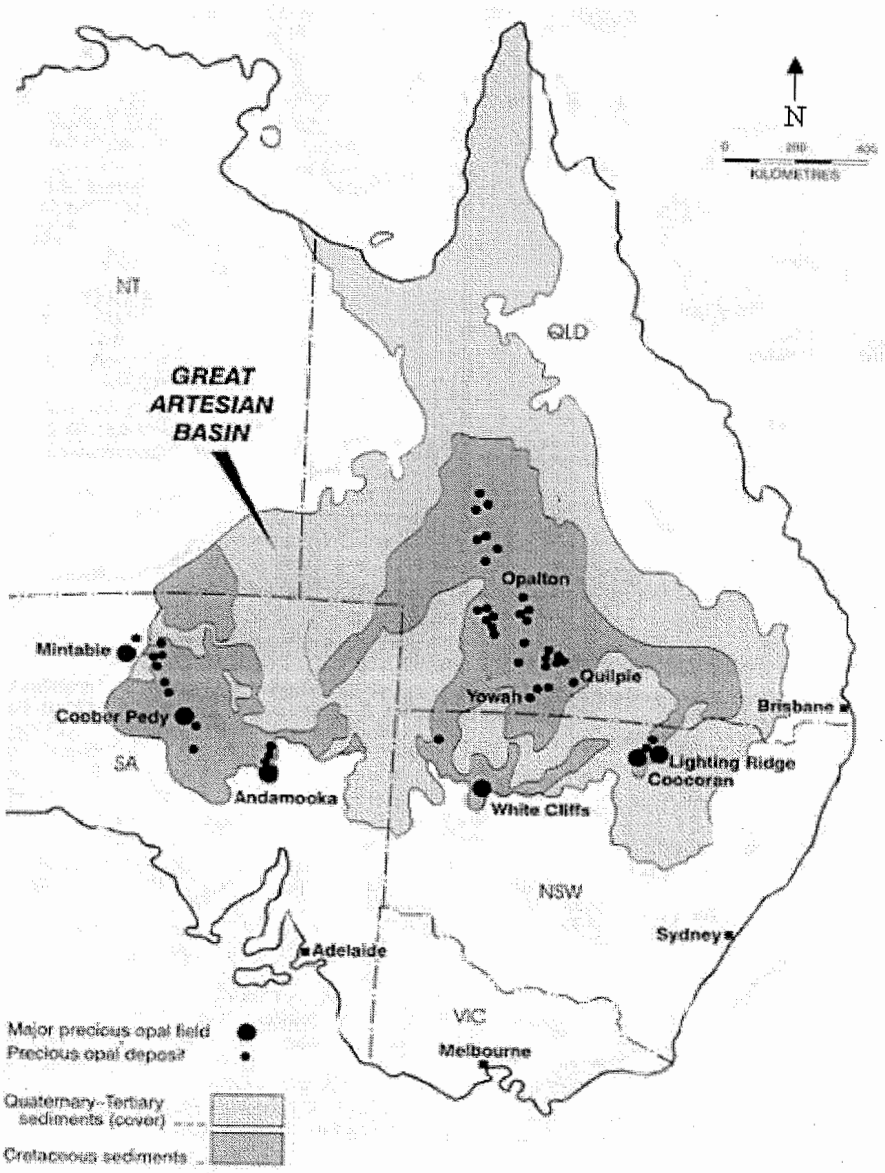

FIG. 1- The Great Artesian Basin with the opal fields (after Townsend 2001).

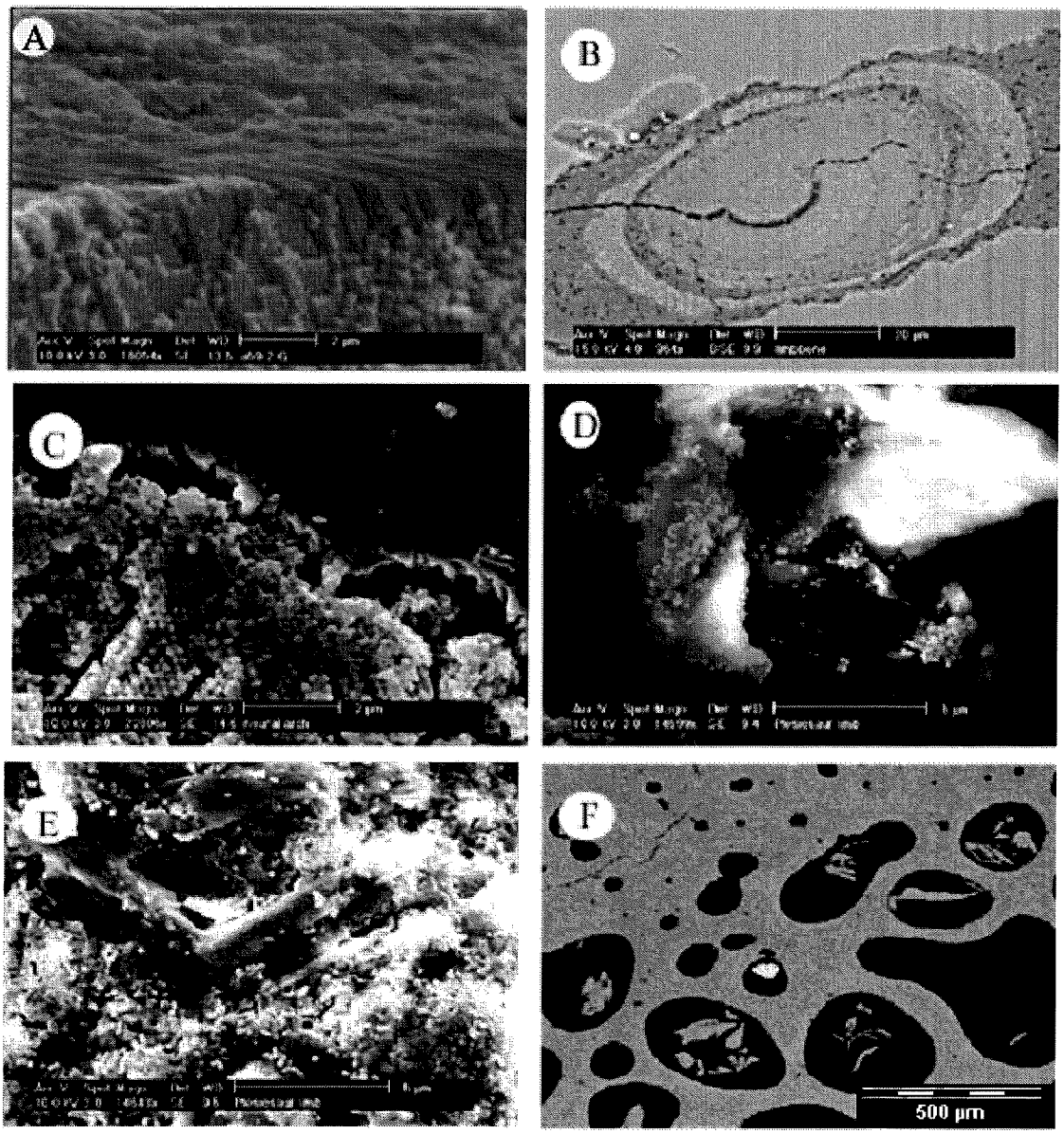

FIG. 2- SEM images of **A)** showing the ordered arrangement of silica spheres in synthetic opals. **B)** Unetched (sample I) showing the Haversian system with growth rings and cracks. Etched (sample K) SEM image showing the space needed for opal formation **(C).** SEM image of etched sample K showing the presence of kaolinite roses **(D)** and loosely packed spheres in bone cavity **(E).** **F)** Dolphin Ca elemental map showing both compact and spongy bone and organic matter within the osteon.

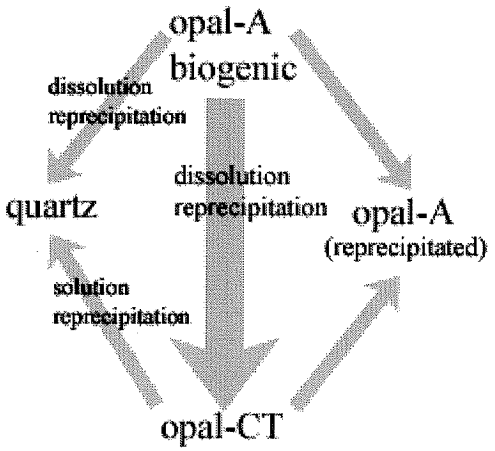

FIG. 3- Phase transformation of silica in deep sea sediments.

The thicker the arrow, the more common the transformation (after Carson 1991).

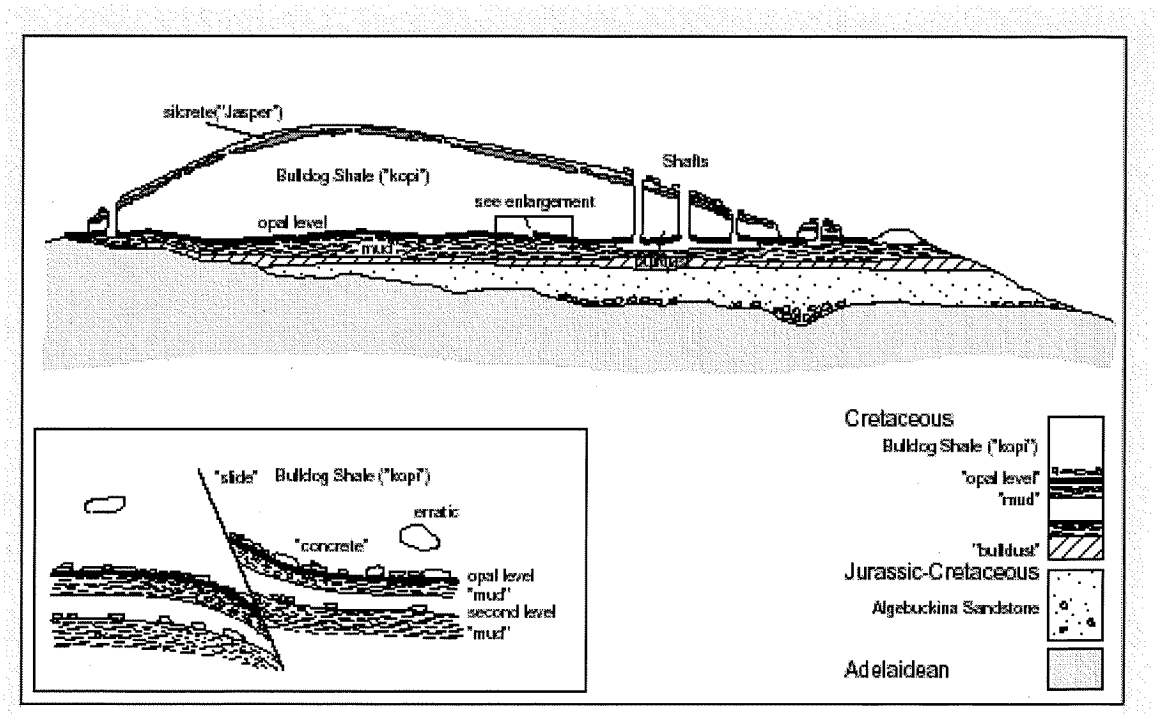

FIG. 4- Schematic cross section of opal lithology/stratigraphy of Andamooka

(after Barnes and Townsend 1990).

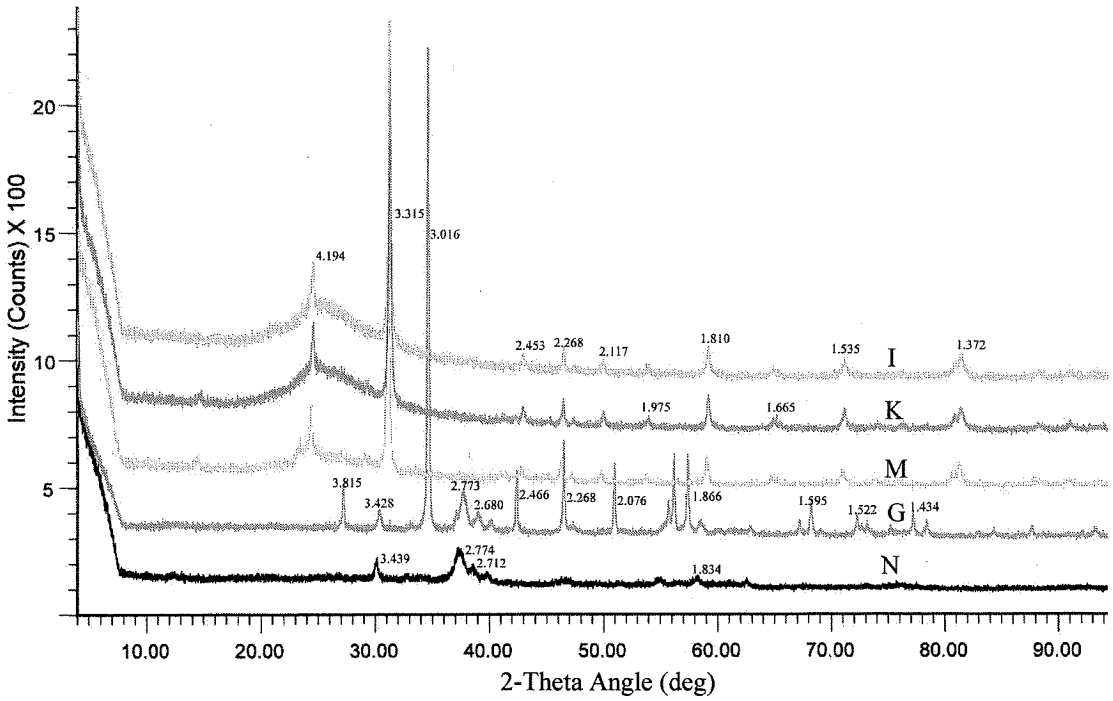

FIG. 5- The X-ray diffraction traces for the bone samples. For clarity, the patterns are displaced 200 CPS from one another. See Table 1 for sample description.

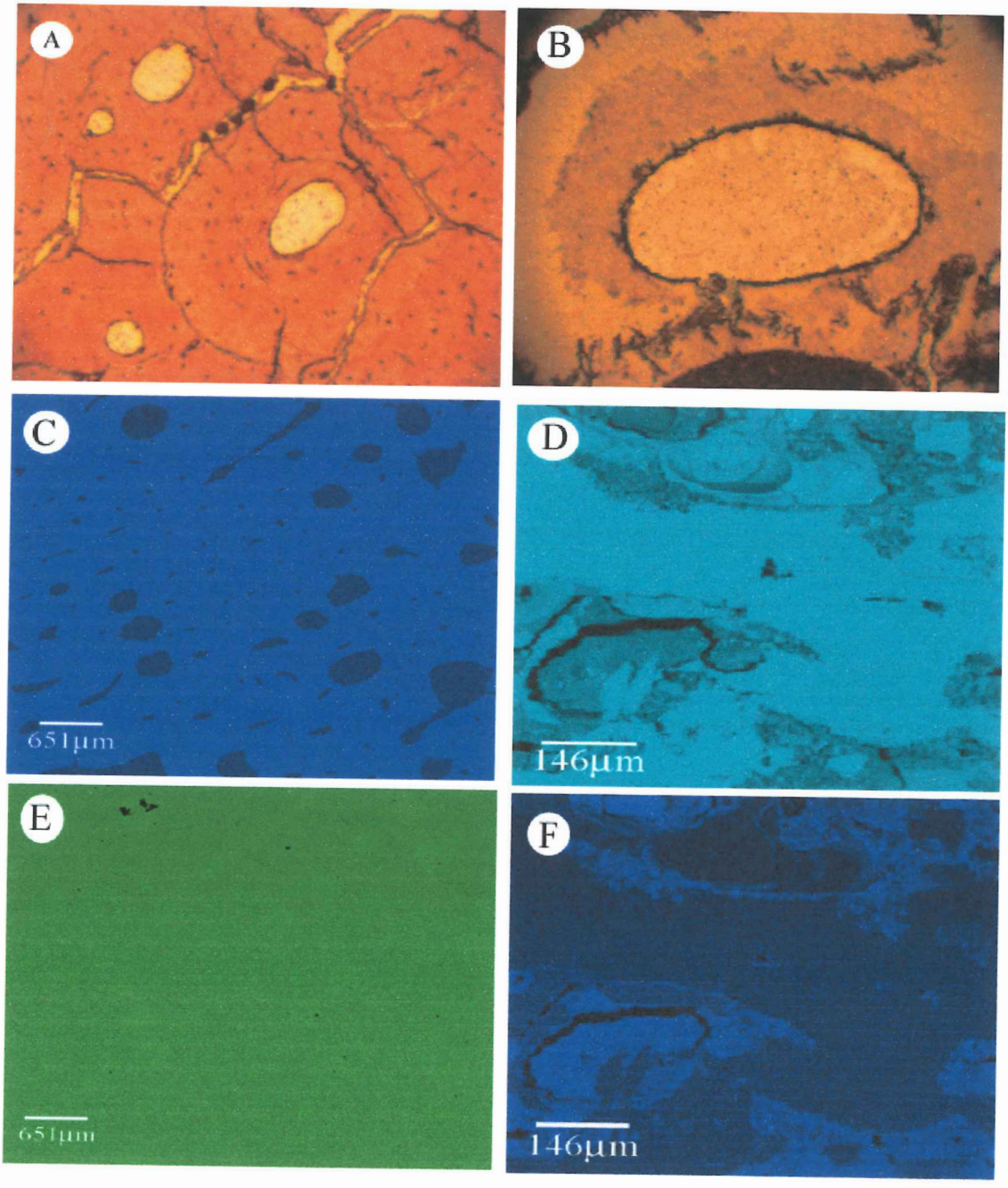

FIG. 6- Ichthyosaur bone (sample H) thin section optical images taken at 20,000x **(A)** along with P **(C)** and Ca **(E)** elemental maps. Opalised plesiosaur neural arch (sample K) thin section optical images taken at 20,000x **(B)** along with Si **(D)** and Al **(F)** elemental maps.

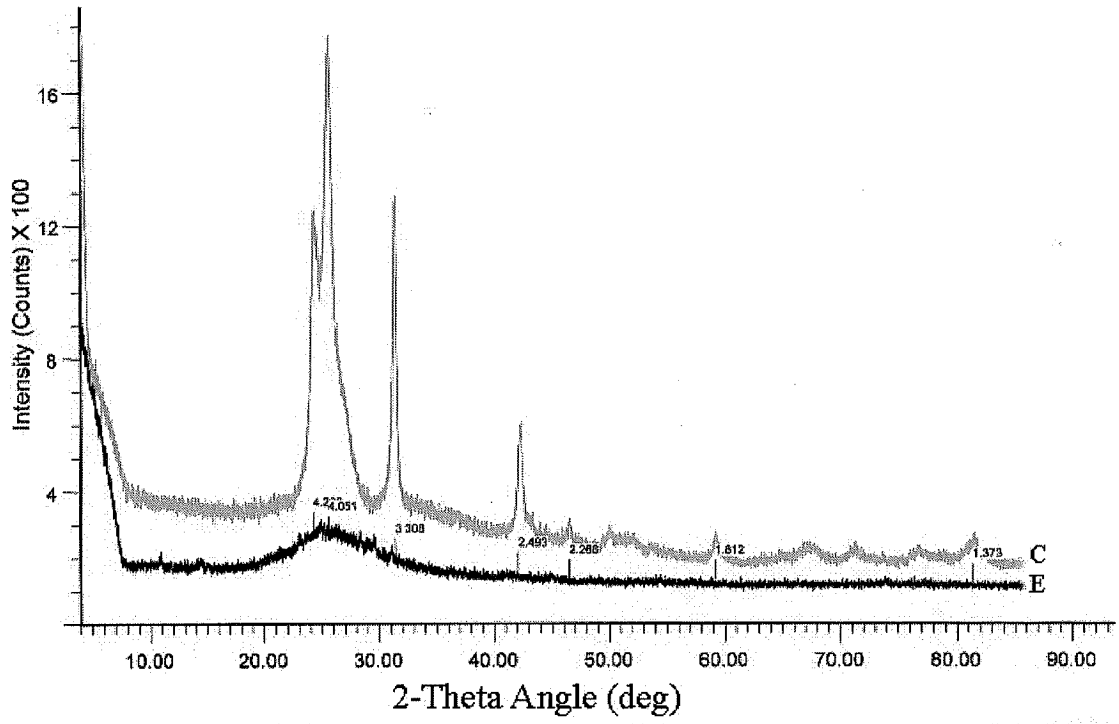

FIG. 7- X-ray diffraction pattern of volcanised opal replacing wood from Nevada (C) and a opalised wood from White Cliff (E). For clarity, the pattern of C is displaced upwards by 5 CPS units.

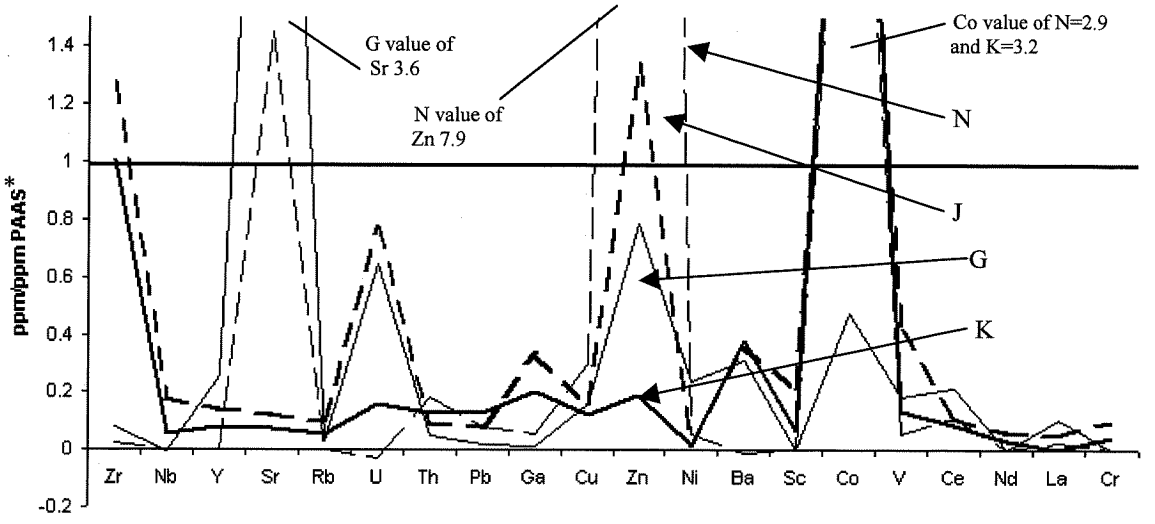

FIG. 8- PAAS normalized rare earth elements (ppm/ppm) of ichthyosaur bone from Moon Plain (G), opalised plesiosaur miscellaneous fragment (J), opalised plesiosaur neural arch (K) and modern dolphin bone (N). *PAAS values from Taylor and McClennan 1985.

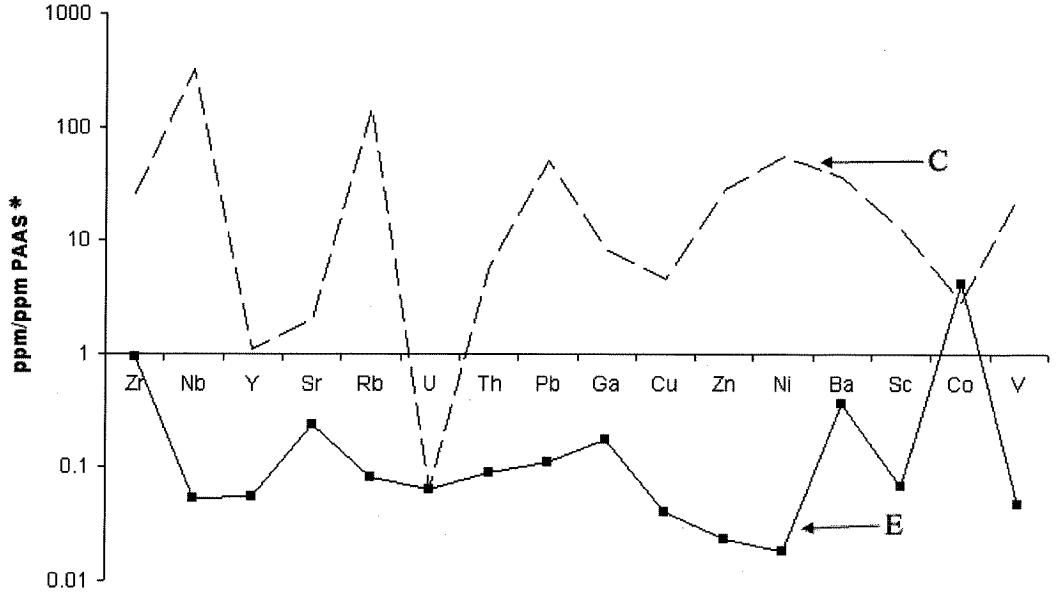

FIG. 9- PAAS normalized rare earth elements (ppm/ppm) of opalised wood from Nevada (C) and from White Cliff (E). For clarity, the graph is in logarithmic scale. *PAAS values from Taylor and McClennan 1985.

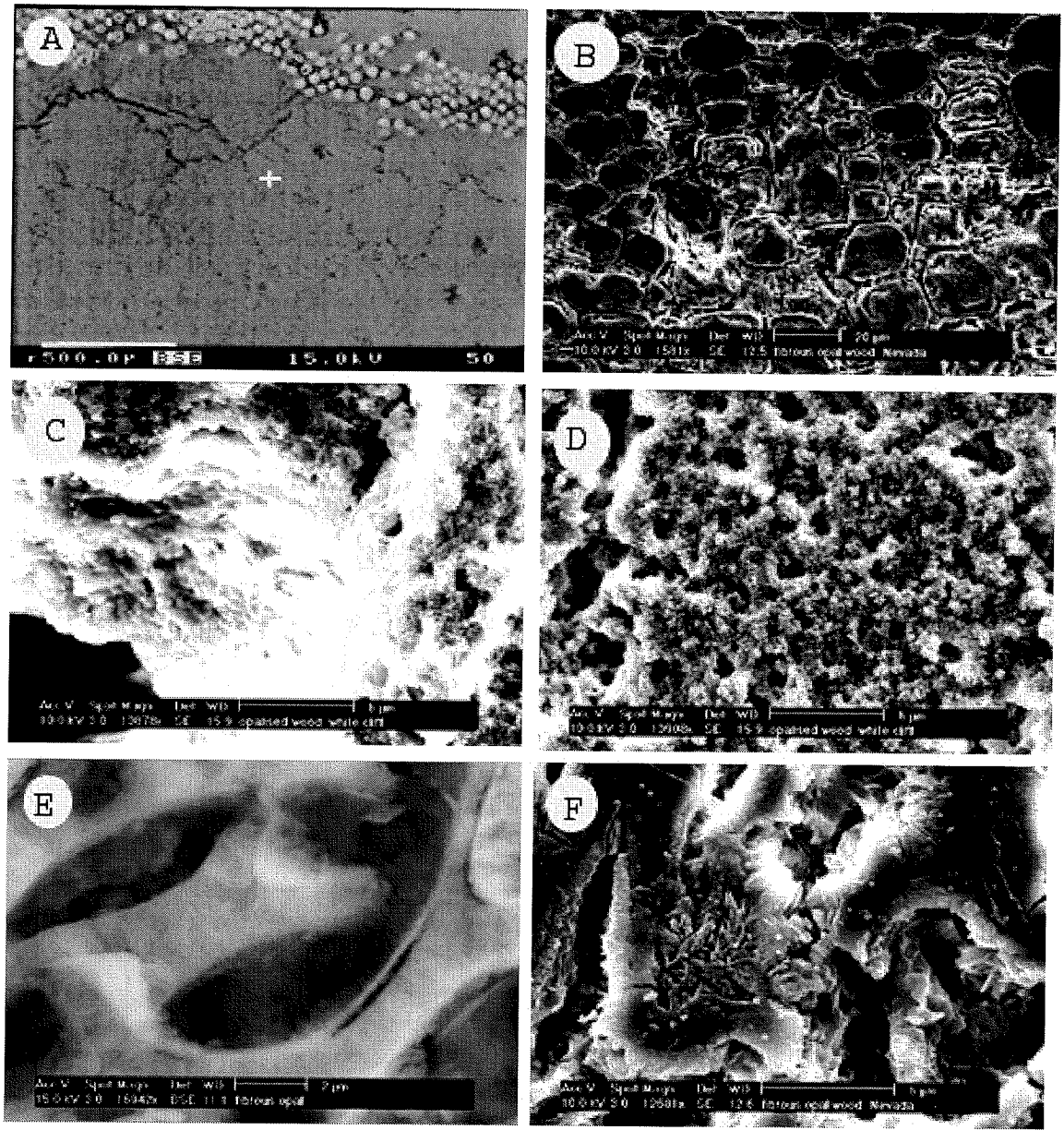

FIG. 10- **A)** Backscatter image of pyrite located on the outer most of the cell structure in sample D. **B)** Unetched (sample B) thin section SEM image showing the cell wall of continuous irregular framework of silica coated with silica spheres. In the SEM image of the etched polished block of sample E, the cell structure was retained away from the fault **C)** and near the fracture the silica spheres are quite porous **D).** **E)** SEM images of tabular crystals of opal-CT in the etched polished block of sample B.

TABLES

TABLE 1- Summary of the samples examined in the study.

sample no	Description	"State"	Location/ Formation	Petrologic thin section	XRD
A	wood opal	opalised	Nevada, USA	Dominant-Am Traces-Trd, carbonate	Trd, O
B	fibrous opal	opalised	Columbus mining district, Nevada, USA	Dominant-Am Traces: Trd (very fine)	Trd, O
C	opal replacing wood	opalised	Columbia district, Nevada, USA	Dominant-Am Traces: Qtz (Trd and/or Crs)	Trd, Qtz, O, Crs
D	fossilised wood	fossilised	Coober Pedy, SA/Bulldog Shale	Dominant-Am, Qtz Traces-tridymite	Trd, Cal, Py
E	opalised wood	opalised	White Cliffs	Dominant-opaline Am Traces-chalcedony	O, Py, Crs
F	opalised shell	opalised	White Cliffs?		Qtz, Gp, Cal
G	Ichthyosaur limb cf *Platypterygius longmani*	fossilised	Moon Plain, 40 km N of Coober Pedy, SA		Cal, Ap
H	icthyosaur	fossilised	Lyme Regis, Dorset, England		Cal, Ap, Qtz
I	Plesiosaur limb	opalised	Andamooka/ Bulldog Shale		Qtz, Ap, O, Py
J	Plesiosauroidea indet miscellaneous fragment	opalised	Andamooka opal field, SA/Bulldog Shale		Qtz, Ap, O
K	Plesiosauroidea indet neural arch fragment	opalised	Andamooka opal field, SA/Bulldog Shale		Qtz, Ap, O
L	Plesiosauroidea indet rib/girdle fragments	opalised	Andamooka opal field, SA/Bulldog Shale		Qtz, Ap, O
M	Plesiosauroidea indet limb/rib fragments	opalised	Andamooka opal field, SA/Bulldog Shale		Qtz, Ap, O
N	Dolphin rib bone	modern	Fowlers Bay, Australia		Ap

NOTE: Tridymite (Trd); Quartz (Qtz), Calcite (Cal), Pyrite (Py), carbonate hydroxylapatite (Ap), Opal (O), Gypsum (Gp), Cristobalite (Crs), Amorphous SiO_2 (Am)

TABLE 2- The results of the major and trace element analyses for selected samples.

	C	D	E	F	G	H	I	J	K	N
SiO2 %	84.58	4.0	91.8	87.7	2.27	0.93	91.87	88.59	92.69	0.15
Al2O3 %	0.26	0.1	2.1	2.9	0.76	0.21	2.12	4.41	2.02	0.04
Fe2O3(tot) %	0.02	1.6	0.1	0.5	0.93	0.77	0.33	0.58	0.22	0.07
MnO %	0.01	0.5	0.0	0.0	0.59	0.03	0.01	0.01	0.01	0.01
MgO %	0.01	2.0	0.1	0.1	7.42	1.08	0.04	0.26	0.09	1.10
CaO %	1.19	45.6	0.2	1.7	40.29	46.88	0.10	0.15	0.06	35.41
Na2O %	0.26	0.4	0.3	0.4	0.61	0.91	0.31	0.36	0.28	0.77
K2O %	0.02	0.0	0.1	0.4	0.08	0.02	0.09	0.19	0.07	0.01
TiO2 %	0.00	0.1	0.1	0.6	0.07	0.04	0.12	0.53	0.16	0.02
P2O5 %	0.01	1.0	0.0	0.0	12.30	27.30	0.01	0.01	0.00	26.00
SO3 %	0.05	0.2	0.0	1.2	5.27	1.23	0.01	0.00	0.01	1.43
LOI %	13.78	40.5	4.1	4.7	26.99	14.48	4.16	4.23	3.63	31.88
Total %	100.18	95.8	98.9	100.1	97.57	93.97	99.16	99.30	99.23	96.88
Zr (ppm)	8.2	7.8	199.0	206.0	16.4	26.2	232.4	267.2	211.7	5.5
Nb (ppm)	0.1	0.9	1.7	6.4	-0.1	4.4	2.6	5.7	1.8	0
Y (ppm)	24.9	2.0	1.5	5.2	7	863.4	2.4	3.8	2.1	0
Sr (ppm)	100.2	583.5	47.2	134.4	720.7	3127.6	16.5	25.1	14.7	290.2
Rb (ppm)	1.1	0.6	13.2	14.0	4.9	3.6	10.9	15.3	8.8	0.5
U (ppm)	48.1	2.4	0.2	1.0	2.0	56.1	1.7	2.4	0.5	-0.1
Th (ppm)	2.4	2.4	1.3	3.6	0.7	5.6	1.0	1.3	1.9	2.7
Pb (ppm)	0.4	1.3	2.2	6.4	0.4	4.6	2.6	1.6	2.6	1.6
Ga (ppm)	2.4	0.0	3.5	5.6	0.3	-0.3	3.2	6.6	4.1	1.1
Cu (ppm)	11.0	0.0	2.0	5.0	8.0	0.0	4.0	8.0	6.0	15.0
Zn (ppm)	3.0	11.0	2.0	3.0	67.0	104.0	15.0	114.0	16.0	678.0
Ni (ppm)	1.0	6.0	1.0	2.0	13.0	6.0	2.0	1.0	1.0	3.0
Ba (ppm)	18.0	79.0	239.0	214.0	204.0	315.0	259.0	236.0	248.0	-6.0
Sc (ppm)	1.3	#	1.1	3.5	#	42.0	1.3	3.4	1.1	#
Co (ppm)	8.0	8.0	97.0	23.0	11.0	25.0	7.0	67.0	75.0	67.0
V (ppm)	6.0	27.0	7.0	52.0	28.0	10.0	28.0	61.0	20.0	8.0
Ce (ppm)	7.0	17.0	6.0	13.0	17.0	1215.0	6.0	9.0	7.0	9.0
Nd (ppm)	5.0	#	0.0	3.0	0.0	670.0	0.0	2.0	1.0	#
La (ppm)	3.0	0.0	1.0	3.0	4.0	561.0	0.0	2.0	0.0	1.0
Cr (ppm)	6.0	#	3.0	12.0	#	2.0	12.0	11.0	5.0	#

Note: # Not analysed because of problems caused by high Ca and/or P.

LOI – Lost On Ignition.